

Structure and Composition of Near-Surface Layers in the Ion-Implanted NiTi Alloy¹

A.D. Pogrebnjak^{***}, S.N. Bratushka^{*}, and N. Levintant^{***}

^{*}Sumy Institute for Surface Modification, PO BOX 163, 40030 Sumy, Ukraine,
Phone: +380-54-78-39-86, E-mail: apogrebnjak@simp.sumy.ua

^{**}Sumy State University, 2, R-Korsakov str., 40007, Sumy, Ukraine, E-mail: alexp@i.ua

^{***}Institute of Fundamental Technological Research, Warsaw, Poland

Abstract – The surface layer of an equiatomic TiNi alloy, which exhibits the shape memory effect in the martensitic state, is modified with high-dose implantation of 65-keV N⁺ ions (the implantation dose is varied from 10¹⁷ to 10¹⁸ ions/cm²). TiNi samples are implanted by N⁺, Ni⁺-N⁺, and Mo⁺-W⁺ ions at a dose of 10¹⁷-10¹⁸ cm⁻² and studied by Rutherford backscattering, scanning electron microscopy, energy dispersive spectroscopy, X-ray diffraction (glancing geometry), and by measuring the nanohardness and the elastic modulus. A Ni⁺ concentration peak is detected between two maxima in the depth profile of the N⁺ ion concentration. X-ray diffraction (glancing geometry) of TiNi samples implanted by Ni⁺ and N⁺ ions shows the formation of the TiNi (B₂), TiN and Ni₃N phases. In the initial state, the elastic modulus of the samples is $E = 56$ GPa at a hardness of $H = 2.13 \pm 0.3$ GPa (at a depth of 150 nm). After double implantation by Ni⁺-N⁺ and Mo⁺-W⁺ ions, the hardness of the TiNi samples is 2.78 ± 0.95 GPa at a depth of 150 nm and 495 ± 2.25 GPa at a depth of 50 nm; the elastic modulus is 59 GPa. Annealing of the samples at 550 °C leads to an increase in the hardness to 4.44 ± 1.45 GPa and a sharp increase in the elastic modulus to 236 ± 39 GPa. A correlation between the elemental composition, microstructure, shape memory effect, and mechanical properties of the near-surface layer in TiNi is found.

1. Introduction

The passage of medium-energy ions through solids is known to be accompanied by their scattering by host atoms and electrons [1, 2], which results in the retardation of ions, a change in the ion motion direction, the displacement of host atoms from lattice sites, the accumulation of impurities in the target, sputtering of the material surface, atomic mixing, the formation of a concentration profile of implanted ions, and the formation of new phases. These factors substantially affect the physicochemical and chemical properties of implanted materials [1–4]. High-dose intense implantation leads to a shift in the maximum in the concen-

tration profile of implanted ions to the surface because of intensified scattering processes [3, 4]. High-dose intense implantation is considered to be ion implantation such that the dose accumulation rate is about 1016 cm⁻²/min and the concentration of implanted ions is several tens (up to 100) of atomic percent [5–7].

The application of high-dose intense implantation leads to an increase in the ion (mainly N⁺ ion) penetration depth; intensified scattering of the surface layer; a shift in the maximum, concentration, and shape of the concentration profile; and many other processes that are weakly pronounced during low-intensity ion implantation at low doses (several units of atomic processes) of implanted ions [1, 2, 5]. On the other hand, TiNi-based alloys belong to the group of materials in which a high-temperature phase with a B₂ structure undergoes a shear or martensitic phase transformation as the temperature changes or a stress is applied. The atomic restructuring in TiNi-based alloys is accompanied by both martensitic anelasticity effects and a change in their surface state, which is caused by the complex structure of the martensite phase in them [8–11]. As a result, a developed martensitic relief with a large number of various interfaces appears, which should affect both the electrochemical and corrosion properties and the plasticity and strength properties of these materials. As a method of surface alloying, ion implantation of a surface can strongly affect the structural parameters and stability of the B₂ phase in the near-surface layers and, hence, the following set of its properties: the martensite transformation temperature, the martensite anelasticity parameters, the shape memory effect (SME), and superplasticity. As a result, it can change the deformation relief, the cracking conditions, and the electrochemical and corrosion properties [12–18]. Therefore, double implantation of N⁺ and Ni⁺ ions into TiNi is of particular interest, since the implantation of Ni⁺ ions changes the equiatomic composition of the alloy and in combination with N⁺ ions, hardens the surface layer and correspondingly, modifies the physicochemical and chemical properties [18–20]. The effect of N⁺ ions on the mechanical properties of steels and alloys is well known. The alloying of steels and alloys with elements such as W and Mo is widely used to improve their mechanical

¹ This work funded by the ISTC Project K-1198. The authors are also thankful to A.P. Kobzev (Joint Institute for Nuclear Physics, Dubna, Moscow Red.) for his help in RBS measurements.

properties; therefore, it is interesting to perform implantation of Mo⁺ and W⁺ ions at high doses. The purpose of this work is to study the depth profile of the elemental composition of the implanted layer, the structure and morphology of the TiNi alloy surface, and the mechanical properties of the alloy implanted by high doses of N⁺ ions (10¹⁷–10¹⁸ cm⁻²) and subjected to double implantation of N⁺, Ni⁺ + N⁺ and W⁺ + Mo⁺ ions at doses ranging from 5 × 10¹⁷ to 10¹⁸ cm⁻².

2. Methods of analysis and coating application

We analyzed equiatomic TiNi (51.5% Ni) alloy samples 22 × 5.4 × 0.25 mm in size. In the initial state, the samples were vacuum annealed at 803 K for 30 min followed by slow cooling. After cooling, the sample surfaces were etched with a mixture of 10% HClO₄ and 90% acetic acid. The N⁺ ion implantation of the TiNi samples was performed on a semi-industrial IMJON (Warsaw) implanter at doses of 1 · 10¹⁷, 5 · 10¹⁷, and 10¹⁸ cm⁻² at a current density of 0.8–1 mA. The implantation of Ni⁺ and Mo⁺ + W⁺ ions was carried out using a vacuum-arc Diana source at a voltage of about 60 kV, a dose of 5 · 10¹⁷ cm⁻², and a substrate temperature of less than 250 °C. Irradiation was performed at a pressure of ~ 10⁻³ Pa. The pulse duration was 200 μs, the pulse repetition frequency was 50 Hz, and the nitrogen concentration in TiNi was determined from the “eating away” in its energy spectrum. The phase-transformation temperatures were determined with a Pyris-1 differential scanning calorimeter, and the elemental composition of the samples was determined by the following methods: Auger electron spectroscopy on a PHI-660 (Perkin-Elmer) device, scanning electron microscopy on a Selm (Sumy, Ukraine) microscope equipped with EDS and WDS microanalyzers and on a Perkin-Elmer microscope, and Rutherford backscattering of ions (2.012-MeV proton beams, 2.035-MeV ⁴He ion beams). Rutherford backscattering spectra were analyzed using the standard RUMP and DWBS software packages [21–23] to construct the depth profiles of elements (Ni⁺, Mo⁺, W⁺ ions). Ions backscattered at an angle of 170° were detected using a surface barrier detector with an energy resolution of 20 keV. In addition, we used a Neophot-2 optical microscope. To measure the mechanical properties and SME, we used a diamond pyramid (Brinell) microindenter with a side of 40 nm at a load of 4, 7, 10, 13, 16 and 20 N and a Talysurf-5-120 scanning profilometer. The measurements were performed in the initial state and after ion implantation. The microhardness on the surface of a sample and across it was measured with a PMT-3 device at various loads. The nanohardness was measured with a trihedral Berkovich pyramid on a Nano Indenter II (MTS System Corp., Ridge, Tennessee, United States) nanohardness tester. To find the hardness and the elastic modulus at the maximum load, we used the Oliver-Pharr technique [24].

X-ray diffractometry, using the Philips diffractometer type X'Pert in the Bragg-Brentano geometry, was used to identify the phase composition of NiTi alloy samples in both unimplanted conditions and after implantation with nitrogen. CuK_α radiation (wavelength λ is 0.154184 nm) diffracted by the sample was selected by a graphite monochromator. The scanning voltage of the X-ray tube was 40 kV, the current was 25 mA, the exposure time was 10 s and the measured angle, 2θ, was from 25 to 95°. The scanning step was 0.02°. The low temperature X-ray diffraction studies were carried out using the TTK Low-Temperature Camera (Anton Paar). The sample was heated from -50 °C up to +150 °C in argon atmosphere. The measured angle, 2θ, was from 35 to 47° with the scanning step of 0.02°. Lattice parameters were determined by using the Philips X'Pert Plus software for all detected peaks.

Specimens for TEM and HREM (Tecnai G². FEI Company) examinations were prepared by Focused Ion Beam System (FEI QUANTA 3D).

3. Experimental results and discussion

With Auger electron spectroscopy, we also studied the TiNi samples before and after implantation with nitrogen ions (Fig. 1). It is seen that, in the initial state, carbon and oxygen are present near the surface; after sputtering for 15–18 min, only nickel and titanium are present in the NiTi sample and their concentrations are close to the equiatomic composition. After implantation, the nickel concentration in the surface layer

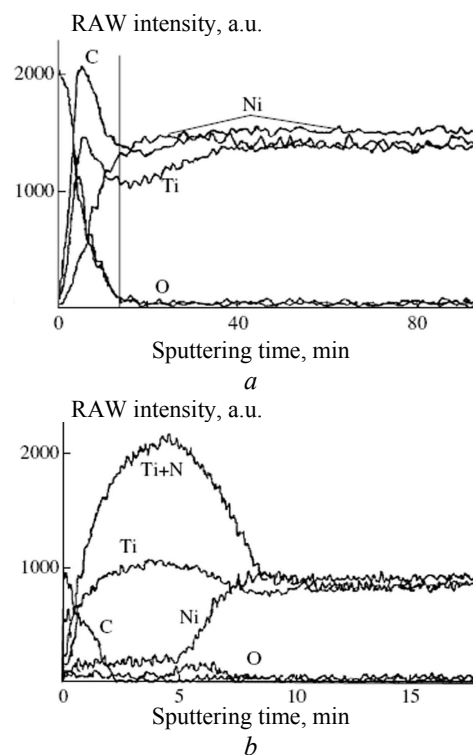


Fig. 1. Auger electron spectroscopy data for (a) unimplanted TiNi samples and (b) TiNi samples implanted at an energy of 65 keV and a dose of 5 · 10¹⁷ ion/cm²

decreases to almost 10 at.% because of sputtering of the surface. Since it is difficult to separate the peaks of nitrogen and titanium ions, we constructed a TiN profile with Auger electron spectroscopy.

This profile indicates that the penetration depth of N^+ ions is about 280–200 nm. After sputtering for 10 min the concentrations of nickel and titanium ions are seen to level off and reach their intrinsic levels (49.9 and 50.1 at.% Ni and Ti in the crystal lattice of the TiNi alloy, respectively).

Figure 2 shows optical microscopy data. They demonstrate a typical martensitic structure and changes in the martensitic structure after implantation.

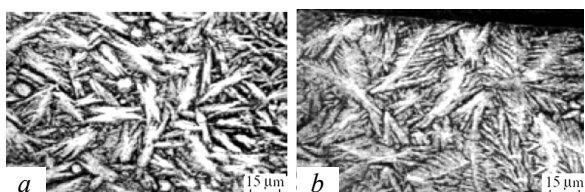


Fig. 2. Optical micrographs of (the cross section of a TiNi alloy with a martensitic structure and SME: *a* – before; *b* – after ion implantation

Figure 3 shows the results of loading and unloading (at loads of 4 and 7 N) of the samples before and after implantation at doses of $5 \cdot 10^{17}$ – 10^{18} cm^{-2} . The TiNi samples implanted by N^+ ions are seen to have a higher (by 15–20%) hardness than the initial samples. The changes in the SME (Fig. 4) demonstrate that the implanted TiNi alloy exhibits an indentation with a higher hardness after recovery as a result of healing to 75 °C. In other words, all mechanical changes related to the SME and mechanical properties (hardness) are interrelated with the elemental composition and micro-structure of the material. Among the light elements, only oxygen exhibits a peak: however, oxygen is located near the sample surface and the eating away is caused by nitrogen.

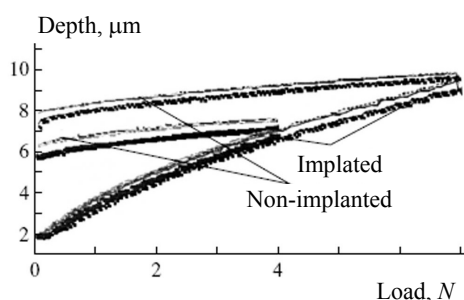


Fig. 3. Indentation curves for implanted and unimplanted TiNi samples exhibiting SME recorded at various loads

Although titanium is seen to be distinguished from nickel and iron, light impurities are not detected. The surface layer of the implanted sample has a significant concentration of nitrogen and oxygen and the characteristic eating away is observed in the spectrum of TiNi implanted sequentially by nitrogen and nickel. We used a standard computer program and determined the nitrogen concentration from the eating away in the spectrum and plotted element-concentration profiles.

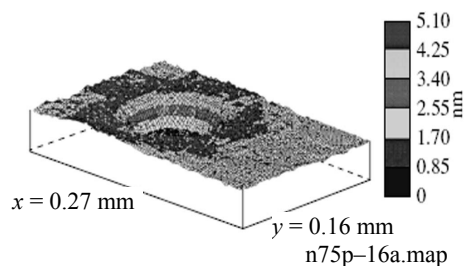


Fig. 4. SME measurements (with a scanning profilometer) on a TiNi sample after heating to 75 °C

The eating away appears when a light element is added to a heavy-element matrix. The yield in a layer containing a light element decreases in proportion to a decrease in the heavy-element concentration. If the light-element concentration increases to 100%, a pure light-element layer forms. Therefore, we can easily determine the error in determining the concentration of nitrogen ions; it was found to be 5 at.%. The error in determining the nickel concentration for concentration profiles was 1.2 at.%. The nickel profile was plotted beginning from 50 at.%. This point was taken as an initial point, since the titanium or nickel concentration in the initial state is about 50 at.%. When analyzing the profile of N^+ ions in TiNi (Fig. 5), we see that the nitrogen profile has a double-humped shape: one concentration maximum is located near the surface (the maximum concentration is about 36 at.%), and the second peak is located at a depth of more than 130–150 nm (133 at. Å² and has a lower concentration (27 at.%). In the valley between the two nitrogen concentration maxima, the concentration of Ni^+ ions is maximal (about 20 at.%).

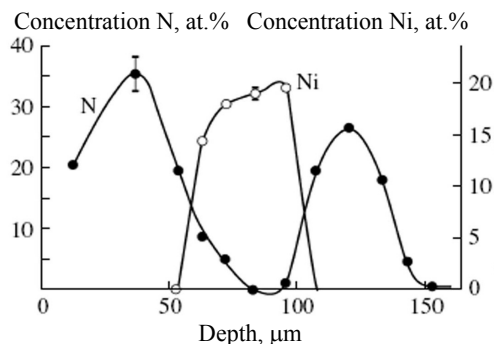


Fig. 5. Depth profiles of the element concentrations obtained from energy spectra of the TiNi sample surface after double implantation of N ions at a dose of 10^{18} cm^{-2} and Ni ions at a dose of $5 \cdot 10^{17} \text{ cm}^{-2}$

Moreover, preliminary SIMS (secondary-ion mass spectrometry) studies also demonstrate the formation of a double-humped nitrogen concentration profile. However, the nitrogen concentrations in the maxima differ slightly from the RBS data, which is caused by the higher threshold of delegability of SIMS ($\sim 10^{-5}$ at.%) [22–23].

The X-ray diffraction patterns of the ion-implanted NiTi alloy against the temperature are shown in Fig. 6. From the results obtained it can be seen that alloys at

20 °C exhibit the three phases: the dominating B19'-phase and a small amount of the R2 and B2 phases.

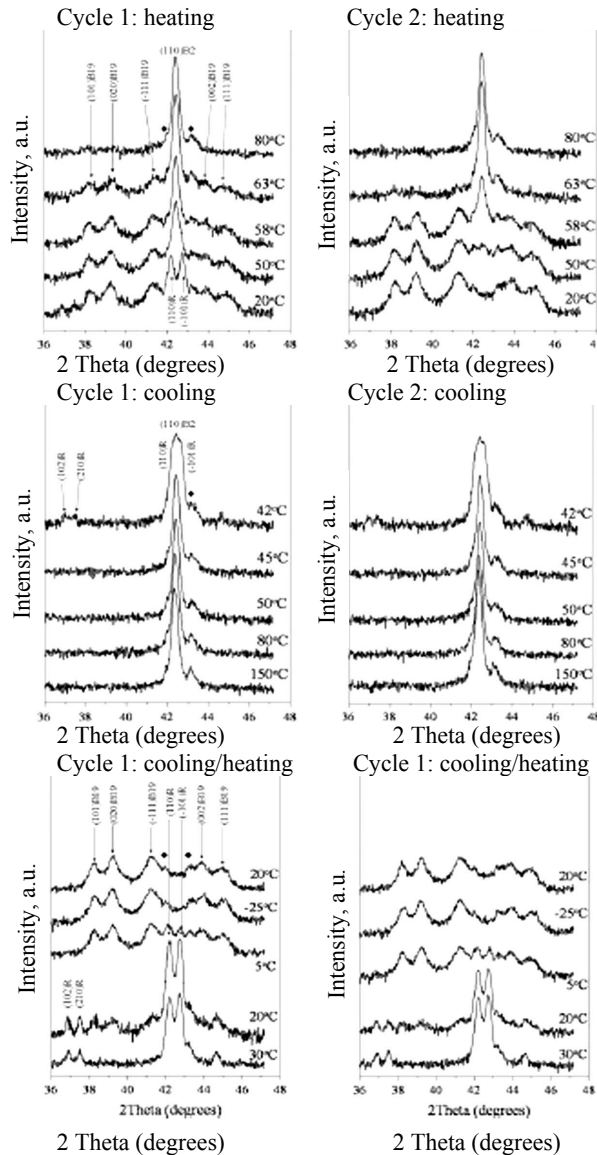


Fig. 6. Recorded X-ray diffraction patterns versus temperature of ion-implanted NiTi alloy at a fluence of 10^{18} cm^{-2} and energy 50 keV

The appearance of austenite phase (crystalline, nanocrystalline and/or amorphous-like) may be related to structural changes in the NiTi alloy during the ion implantation process and to high temperature of target. Appearance of the R-phase, similar to the results obtained for annealed materials, may be induced by high temperature of target. An increase of temperature in the material results in an increasing fraction of the B2-phase. As follows from Fig. 6 the diffraction patterns of this B19'-phase do not vary up to 65 °C. Above this temperature an increasing fraction of the B2-phase and a distinctly decreasing fraction of the B19' one were observed. The B19' \rightarrow B2 phase transformation finishes above a temperature of 80 °C. The X-ray diffraction patterns obtained for the highest temperatures

(from 80 to 150 °C) contain only reflections from the B2-phase. Lowering the temperature up to about 41 °C, besides still existing B2-phase, the R-phase appears. From the results obtained it can be seen that the R \rightarrow B19'-phase transformation starts from a temperature of 25 °C and finishes about 25 °C. Along with the decreasing temperature, besides the dominating B19'-phase, a small amount of the B2-phase was detected. Such phase composition was also observed for the material at 20 °C on the start and finish of the second thermal cycle. The broad structure of this diffraction peak may testify that still some amount of the amorphised and/or nano-crystalline B2-phase is present in the alloy. It should be noted that from the results obtained there is no evidence for TiN and Ti₂Ni compound formations.

The concentration and the type of defects produced in materials during ion implantation depend on the implantation conditions, such as implantation temperature, fluence and fluence rate. Physical processes, which arise during interaction of accelerated ions with a crystal as a result of ion implantation, apart from the ionization of parent atoms and insertion of foreign ones, include formation of post-implanted crystal defects. It is very well known that when a material is uniformly irradiated by ions, isolated damaged regions are created in the first stage. Depending on the size of these regions and the irradiation fluence, the damaged regions start to overlap and a continuous disordered (saturated at the critical fluence) layer is formed. The disordered material contains large concentration of vacancy clusters, implanted impurity and other defects mainly within this material, but they are also present in transition zones. Naturally, the maximum of post-implanted defects distribution is closer to the crystal surface than the maximum of impurity concentration profile.

In the process of nitrogen ion implantation with the fluence 10^{18} cm^{-2} and 50 keV of energy, the well-defined double-layer structure with different microstructure as well as different phase and chemical composition was formed (Fig. 7). During ion implantation, collisions between the incident ions and the NiTi-target atoms lead to the formation of near-surface amorphized layer (A-layer, Figs. 7 and 8, a) and the extended defects in the crystalline structure of bulk material (D-layer in Figs. 7, a and 8, b; Bulk in Fig. 7, a).

The transition zone of a damaged region is wide and its composition changes gradually from totally amorphized Ti-rich material (heavily damaged and nano-crystalline) to Ni-rich crystalline (A1 and A2 regions in A-layer in Figs. 7, b, c). Amorphous-like layer contains some amount of crystalline inclusions within its bulk (P1 and P2 regions in Fig. 8, a), mainly near a bottom boundary of the transition zone (P2-region).

This confirms the fact that the amorphization process occurs faster from the depth of maximum damage regions towards the sample surface than in its bulk.

Due to differential strain between the undamaged and damaged layers, many cracks appear in this region. In the depth of 80–160 nm the material has a defected crystalline microstructure (Fig. 8, *b*).

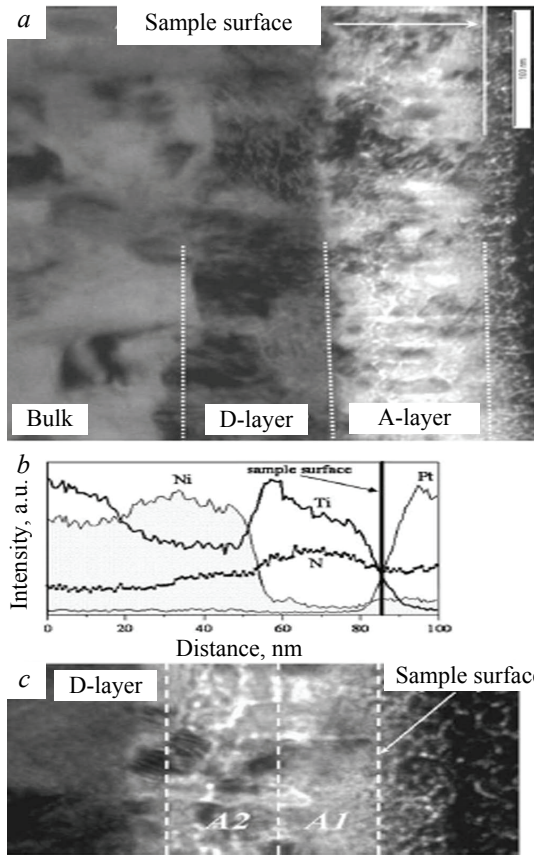


Fig. 7. (a) Bright-field image of the ion-implanted NiTi alloy demonstrating the structure and (b), (c) chemical composition changes in near-surface layers

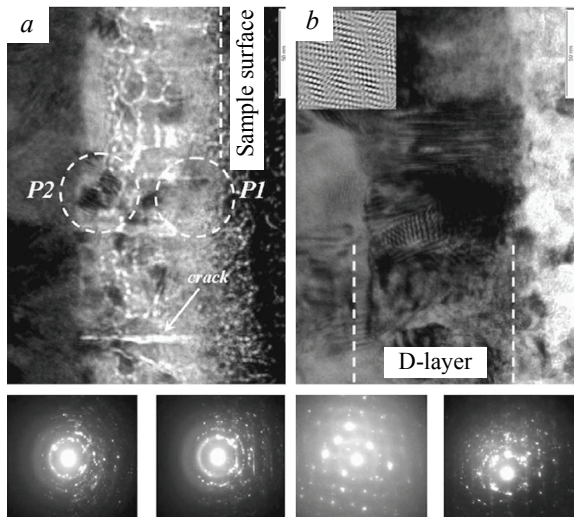


Fig. 8. Bright-field image of the ion-implanted NiTi alloy demonstrating the details of structural changes in near-surface layers

The hardness (H) and Young's modulus (E) data change correspondingly. Their values were determined at various depths (see Tables 1, 2). The hard-

ness is seen to increase from 2.13 ± 0.13 to 2.78 ± 0.95 GPa at a depth of 150 nm. The elastic modulus varies from $E = 56 \pm 2$ to 59 ± 11 GPa. After annealing at 550°C for 2 h, these values increase sharply: $H = 4.11 \pm 0.35$ GPa, $E = 289 \pm 81$ GPa. Small differences between the hardnesses and elastic moduli of the initial and implanted and annealed samples are also detected at a depth of 50 nm. Upon implantation, we have $H = 4.96 \pm 2.26$ and $E = 59 \pm 8$ GPa; after annealing, we have $H = 4.44 \pm 1.45$ and $E = 236 \pm 39$ GPa (the elastic modulus increases by a factor of almost 4.5). Figure 9 shows the TiNi sample surface after double implantation by N^+ and Ni^+ ions. The surface is rather rough ($a = 0.8\text{--}1.2\ \mu\text{m}$) due to sputtering mainly by nitrogen atoms.

Table 1. Hardness and elastic modulus of TiNi samples at a depth of 150 nm

	Sample	E , GPa	H , GPa
1	Initial	56 ± 2	2.13 ± 0.30
2	W + Mo	59 ± 11	2.78 ± 0.95
3	W + Mo. after annealing	298 ± 81	4.11 ± 0.35

Table 2. Hardness and elastic modulus of TiNi samples at a depth of 50 nm

	Sample	E , GPa	H , GPa
1	Initial	56 ± 4	2.74 ± 0.30
2	W + Mo	59 ± 8	4.95 ± 2.26
3	W + Mo. after annealing	236 ± 39	4.44 ± 1.45

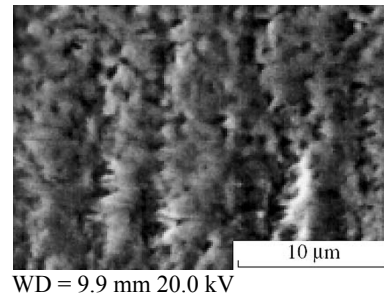


Fig. 9. TiNi sample surface implanted by nitrogen and nickel

This surface was subjected to electron-probe microanalysis. The following elements were detected in the near-surface layer (Fig. 9): N (~ 2.1 at.%), O (~ 5.61 at.%), C (~ 0.58 at.%), Ni (~ 49.43 at.%), and Ti (~ 41 at.%). To detect Ti, we used another detector. The low (as compared to the RBS data) titanium concentration is caused by the larger depth of SEM as compared to EDS (which is $2.2\ \mu\text{m}$); moreover, the nitrogen ion range is at most 300 nm at the energies (60–70 keV) used in our experiments. Upon implantation, the elastic modulus increases insignificantly; however, after heat treatment, it increases to 236 ± 39 or 289 ± 80 GPa (i.e., by a factor of 4–4.5 compared to the initial state).

4. Conclusions

We showed that the sequential double implantation of N^+ and Ni^+ ions into nitinol (TiNi) leads to the for-

mation of a complex depth profile of the nitrogen concentration, which is caused by the rejection of nitrogen ions from the region of the maximum Ni^+ ion losses (i.e., the region of the maximum Ni^+ ion concentration) to the region of residual tensile stresses. As a result of the implantation of N^+ , Ni^+ , W^+ , and Mo^+ ions, the hardness after implantation increases by 30% compared to the initial state and the hardness after subsequent thermal annealing at 550°C for 2 h increases by a factor of 2.2. The SME changes because of the formation of nitrogen and carbon (carbonitride) layers as a result of N^+ implantation and because of a change in the concentrations of Ti and Ni atoms due to the sputtering of Ni atoms, which is accompanied by a change in the martensite transformation temperature.

The martensitic form of equiatomic NiTi was implanted with N ions with the fluence 10^{18} cm^{-2} and 50 keV energy. To characterize the transformation sequence and transformation temperatures, the DSC measurements were carried out on an unimplanted as well as an implanted material. Both the unimplanted and ion-implanted NiTi alloys transform in two steps ($\text{B2} \rightarrow \text{R} \rightarrow \text{B19}$) in the cooling direction and one-step transition ($\text{B19} \rightarrow \text{B2}$) in the heating process. To verify identifications of martensitic transformations in the NiTi alloys during heating and cooling, the X-ray structural investigations were performed.

The TEM structural characterization reveals the existence of the well-defined double-layer structure with different microstructure as well as different phase and chemical composition in the near-surface region of the ion-implanted NiTi alloy. From the surface to a depth of 80 nm, the sample has an amorphized structure in the form of two sublayers: the first is a Ti- and N-rich nano-crystalline and/or amorphous-like and the second – Ni-rich crystalline. In the depth of 80–160 nm the material has a defected Ti-rich crystalline microstructure and deeper – an unaffected grain structure of the parent material.

References

- [1] Treatise on Materials Science and Technology, Ed. by W.F. Wang, **18**: Ion Implantation. Ed. by J.K. Hirvonen (Academic, New York, 1980; Metallurgiya, Moscow, 1985).
- [2] F.F. Komarov, *Ion Implantation in Metals*, Moscow, Energoatomizdat, 1990 [in Russian].
- [3] A.D. Pogrebnjak and A.M. Tolopa, Nucl. Instrum. Methods Phys. Res. B **52**, 24 (1990).
- [4] A. Pogrebnjak, A. Kobzev, B.P. Gritsenko et al., J. Appl. Phys. **87**, 2142 (2000).
- [5] A.D. Pogrebnjak, A.P. Kobzev, B.P. Gritsenko et al., Jpn. J. Appl. Phys. **38**, 248 (1999).
- [6] A.D. Pogrebnjak, V.A. Martynenko, A.D. Mikhailiev et al., Pis'ma Zh. Tekh. Fiz. **27**, 14, 88 (2001) [Tech. Phys. Lett. **27**, 615 (2001)].
- [7] V.M. Anishchik and V.V. Uglov, *Ion Implantation into Tool Steel*, BGU, Minsk, 2000 [in Russian].
- [8] L.L. Meisner, V.P. Sivokha, Yu.P. Sharkeev, S.N. Kulikov, and B.P. Gritsenko, Zh. Tekh. Fiz. **70**, 1, 32 (2000) [Tech. Phys. **45**, 30(2000)].
- [9] L.L. Meisner, Doctoral Dissertation in Mathematical and Physics, Tomsk, 2004.
- [10] T. Labrande, C. Abromelt, and R. Gotthard, Mater. Sci. Eng. A **438–440**, 521 (2006).
- [11] N. Shevchenko, M.-T. Pham, and M.F. Maitz, Appl. Surf. Sci. **235**, 126 (2004).
- [12] T. Lehnert, S. Tixier, P. Boni, and R. Gotthardt, Mater. Sci. Eng. A **273–275**, 713 (1999).
- [13] J. Humbeek, Scr. Mater. **50**, 179 (2004).
- [14] B. Raniecki and C. Lexcellent, Eur. J. Mech. A/Solids **17–20**, 185 (1998).
- [15] K. Madangopal, Scr. Mater. **53**, 875 (2005).
- [16] D. Chrobak and H. Morawiec, Scr. Mater. **44**, 725 (2001).
- [17] L.L. Meisner, V.P. Sivokha, A.I. Lotkov, and L.A. Derevyagina, Physica B **307**, 251 (2001).
- [18] H. Pelletier, D. Muller, P. Mille, and J.J. Grob, Surf. Coat. Technol. **158**, 309 (2002).
- [19] M.C. Carroll, Ch. Somsen, and G. Eggler, Scr. Mater. **50**, 187(2004).
- [20] N. Levintant, Vacuum **81**, 1283 (2007).
- [21] T. Czeppea, N. Levintant-Zayontsb, Z. Swiatek et al., Vacuum **83**, S214 (2009).
- [22] A.D. Pogrebnjak, S.N. Bratushka, V.V. Uglov et al., Vacuum **83**, S240 (2009).
- [23] A.D. Pogrebnjak, S.N. Bratushka, L.V. Malikov et al., Zh. Tech. Fiz. **79**, 65 (2009).

Pogrebnjak, A. D. Structure and Composition of Near-Surface Layers in the Ion-Implanted NiTi Alloy [Text] / A. D. Pogrebnjak, S. N. Bratushka, N. Levintant // 10th International Conference on Modification of Materials with Particle Beams and Plasma Flows : proceedings. - Tomsk, 2010. - P. 213-219.